On avoiding spurious mesh sensitivity in dynamic finite element analysis of plastic strain localization

Fékri Meftah* — Jean Marie Reynouard**

**L.M.T-Cachan, E.N.S de Cachan / C.N.R.S / Université P. et M. Curie*
61, Avenue du Président Wilson, F-94235 Cachan
meftah@lmt.ens-cachan.fr

***URGC-Structures, Institut National des Sciences Appliquées de Lyon*
20, Avenue Albert Einstein, F-69621 Villeurbanne
Reynouar@gcu-beton.insa-lyon.fr

ABSTRACT. *Failure analysis poses a some challenging problems when the degradation of the continuum into a discontinuum is to be captured. Indeed, the physics of progressive failure and its description in terms of continuum damage mechanics or strain softening plasticity raise a number of fundamental issues. The mathematical formulation of physically unstable phenomena leads to ill posed initial boundary problems. Therefore, the concomitant computational solution strategy is inherently sensitive to incipient failure and is then insufficiently robust to survive loss of stability, uniqueness and hyperbolicity. This paper will focus on the use of gradient plasticity theory as a localization limiter incorporated in beams theories to describe Mode-I failure analyses. The approach will be assessed and illustrated with model examples.*

RÉSUMÉ. *L'amorce de la rupture dans les matériaux fragiles induit une forte localisation des déformations accompagnée par une chute de la capacité portante du matériau communément appelée adoucissement. La prise en compte de ce phénomène dans un modèle de plasticité conventionnelle, en vue d'une modélisation par éléments finis, conduit à une solution dépendant pathologiquement du maillage. Ainsi, la zone de localisation est complètement déterminée par la discrétisation, et une convergence vers une solution unique n'est plus assurée. C'est dans ce contexte que s'inscrit le présent travail. Il est consacré à la mise en œuvre de la théorie de la plasticité avec second gradient du paramètre d'écrouissage dans un modèle multicouches en vue du calcul des structures de type poutres en béton et bétons armé. L'application à des cas de structures sous sollicitations impulsionnelles est présenté pour illustrer et valider l'approche.*

KEY WORDS : *strain localization, dynamic loding, mesh sesitivity, finite element.*

MOTS-CLÉS : *Localisation, déformation, dynamique, sensibilité, maillage, élément fini.*

1. Introduction

The localization of deformations is a physical phenomenon observed in a wide range of engineering materials such as concrete, rock and soils. The successful numerical analysis of this phenomenon requires the use of a regularization technique in order to ensure the well posedness of the initial boundary value problem [LOD°94, PIJ°87, SLU°92a]. In this contribution, we make use of gradient plasticity theory regularization [BOR°92]. The main feature of this theory is the dependence of the yield function upon the Laplacian of an invariant plastic strain measure. Therefore, the plastic consistency condition becomes a partial differential equation. Weak satisfaction of the consistency condition is then assumed together with the equilibrium one to solve the initial boundary value problem of nonlinear dynamics with small deformations.

Independent finite element discretizations of the displacement and the plastic multiplier fields are then used leading to a mixed formulation. Furthermore, the theory incorporates a *characteristic or internal length* parameter that controls bifurcation phenomenon, prevents localization according to discontinuous modes of deformation and allows us to define the width of the localization zone. A multilayered approach based on gradient plasticity and on a simplified beam kinematic is developed [MEF°98, MEF°97]. Its application to concrete beams under impulsive loads is presented to validate and illustrate the numerical model.

2. Incremental formulation

We consider the following set of field equations :

$$\mathbf{L}^T \boldsymbol{\sigma} - \mathbf{R}\,\ddot{\mathbf{u}} = \mathbf{0}\,, \qquad [1]$$

$$\dot{\boldsymbol{\varepsilon}} = \mathbf{L}\dot{\mathbf{u}}\,, \qquad [2]$$

$$f(\boldsymbol{\sigma}, \kappa, \nabla^2 \kappa) = 0\,, \qquad [3]$$

$$\dot{\boldsymbol{\sigma}} = \mathbf{D}^e(\dot{\boldsymbol{\varepsilon}} - \dot{\lambda}\frac{\partial f}{\partial \boldsymbol{\sigma}})\,,\ \dot{\lambda} \geq 0, \qquad [4]$$

which define the elastoplastic initial boundary value problem during associated plastic flow, and where the superimposed dots denote a differentiation with respect to time and the superscript T is the transpose symbol. The momentum equation (Eq.1), the continuity equation (Eq.2) and the flow low (Eq.4) based on normality rule are similar to those used in classical plasticity. The main difference is therefore the dependency of the yield function (Eq.3) upon the second gradient of the history parameter. In the equations mentioned above $\mathbf{R}$ is the density matrix that is equal to $diag[\rho,\rho,\rho]$ with density ρ, $\mathbf{L}$ is a differential operator matrix, $\dot{\boldsymbol{\sigma}}$ and $\dot{\boldsymbol{\varepsilon}}$ are the stress

and strain rate tensors (in vector form), respectively, $\dot{\mathbf{u}}$ is a displacement rate vector, $\ddot{\mathbf{u}}$ the acceleration vector, $\mathbf{D}$ the elastic stiffness matrix, $\dot{\lambda}$ a multiplier being a measure of plastic flow intensity, f the gradient dependent yield function and κ the hardening parameter related to the plastic strain tensor $\dot{\varepsilon}^{p}$ by the strain-hardening hypothesis,

$$\dot{\kappa} = \sqrt{\frac{2}{3}(\dot{\varepsilon}^{p})^{T}(\dot{\varepsilon}^{p})}\,. \qquad [5]$$

If we restrict the analysis to Huber-Mises and Drucker-Prager plasticity, the nonlocal yield function can be expressed as

$$f\left(\sigma,\kappa,\nabla^{2}\kappa\right)=\tau(\sigma)-\bar{\tau}_{g}\left(\kappa,\nabla^{2}\kappa\right)=0 \qquad [6]$$

where $\tau(\sigma)$ is a function of stress tensor invariants and $\bar{\tau}_{g}$ is the uniaxial equivalent stress that is gradient dependent. Those plastic criteria verify the following relation

$$\dot{\kappa} = \eta\,\dot{\lambda} \qquad [7]$$

with η a constant depending on the definition of $\tau(\sigma)$. The gradient dependent yield strength $\bar{\tau}_{g}$ can be given by

$$\bar{\tau}_{g}\left(\kappa,\nabla^{2}\kappa\right)=\bar{\tau}(\kappa)-g(\kappa,l)\nabla^{2}\kappa \qquad [8]$$

where $\bar{\tau}(\kappa)$ is the local uniaxial equivalent stress and g is a weight function depending on the hardening parameter, giving the effective contribution of the nonlocal gradient term and therefore related to the internal length. In fact, this relation can be derived from the former nonlocal theory [PIJ°87] in which the yield strength $\bar{\tau}_{nl}$ in a material point $\mathbf{x}$ is considered as a weighted average of the local yield strength $\bar{\tau}$ over the surrounding volume Ω_{s}

$$\bar{\tau}_{nl} = \frac{1}{\Omega_{s}}\int_{\Omega}\phi(\xi)\cdot\bar{\tau}(\mathbf{x}+\xi)\,\mathrm{d}\Omega = 0\,,\ \text{with}\ \Omega_{s} = \int_{\Omega}\phi(\xi)\,\mathrm{d}\Omega \qquad [9]$$

in which $\phi(\xi)=exp\left(-|\xi|^{2}/2\cdot l^{2}\right)$ is a gaussian weight function and ξ denotes the relative position vector pointing to the infinitesimal volume $\mathrm{d}\Omega$. The parameter l is again the internal length parameter governing the contribution on the yield strength (additional carrying capacity) of the surrounding volume at the given material point $\mathbf{x}$. The gradient formulation can then be derived from this nonlocal theory. The local yield strength is expanded into Taylor series according to

$$\bar{\tau}(\mathbf{x}+\xi) \approx \bar{\tau} + \nabla\bar{\tau} \bullet \xi + \frac{1}{2!}\nabla^2\bar{\tau} \bullet \xi^{(2)} + \frac{1}{3!}\nabla^3\bar{\tau} \bullet \xi^{(3)} + \frac{1}{4!}\nabla^4\bar{\tau} \bullet \xi^4 + \cdots \quad [10]$$

where, ∇^n is the n^{th} order gradient operator, the dot $\bullet$ denotes inner product between n^{th} order tensors and $\xi^{(n)}$ denotes the n factor dyadic product $\xi \otimes \cdots n\text{-}times \cdots \otimes \xi$. By substituting Eq.(10) into Eq.(9) and considering that the domain Ω_s remains small compared to Ω, an exact integration in equation (9) is possible, leading to the vanishing of the odd terms [MEF°97] such that

$$\bar{\tau}_{nl} \approx \bar{\tau} + c_1(l) \cdot \nabla^2\bar{\tau} + c_2(l) \cdot \nabla^4\bar{\tau} + \cdots . \quad [11]$$

The gradient parameters c_i are of the dimension of a length to an even power, so that the internal length scale is present in this gradient formulation. For computational reasons (due to the discretization of the plastic strain field), the higher order terms in expression (11) are neglected such that relation (8) is retrieved; in which the yield strength is made as a function of the cumulated plastic strain κ. The gradient function $c_1(l)$ has also been made dependent on the cumulated plastic strain to take into account nonlinear softening flow [11].

In classical plasticity, the consistency condition $\dot{f}(\sigma,\kappa) = 0$ is combined with the flow low (Eq.4) to determine the plastic multiplier intensity and then an elastoplastic tangent stiffness operator. In gradient plasticity, however, the consistency condition $\dot{f}(\sigma,\kappa,\nabla^2\kappa) = 0$ becomes a partial differential equation making impossible to compute the plastic multiplier explicitly. Therefore, an incremental-iterative algorithm presented in [MEF°97, PAM°94, SLU°92a] has been derived for gradient plasticity. This algorithm requires a weak satisfaction of both motion equation and yield condition (Eqs.1 and 3) at the end of time step $t+\Delta t$:

$$\int_\Omega \mathbf{u}^T \left[\mathbf{L}^T \sigma^{t+\Delta t} - \mathbf{R}\,\ddot{\mathbf{u}}^{t+\Delta t} \right] d\Omega = 0 \quad [12]$$

and

$$\int_\Omega \square f\left(\sigma^{t+\Delta t}, \kappa^{t+\Delta t}, \nabla^2\kappa^{t+\Delta t}\right) d\Omega = 0 \quad [13]$$

respectively, leading to the two variational equations:

$$\int_{\Omega} \delta \mathbf{u}^{\mathrm{T}} \left[\mathbf{R}\, \ddot{\mathbf{u}}^{t+\Delta t} \right] \mathrm{d}\Omega + \int_{\Omega} \delta \boldsymbol{\varepsilon}^{\mathrm{T}} \left[\int_{t}^{t+\Delta t} \mathbf{D}^{\mathrm{e}} \left(\dot{\boldsymbol{\varepsilon}} - \dot{\lambda}\, \mathbf{n} \right) \mathrm{d}\tau \right] \mathrm{d}\Omega = \int_{\partial\Omega} \mathbf{u}^{\mathrm{T}}\, \mathbf{t}^{t+\Delta t}\, \mathrm{dS} - \int_{\Omega} \delta \boldsymbol{\varepsilon}^{\mathrm{T}} \boldsymbol{\sigma}^{t}\, \mathrm{d}\Omega \qquad [14]$$

and

$$\int_{\Omega} \delta\lambda \int_{t}^{t+\Delta t} \left[\mathbf{n}^{\mathrm{T}}\, \mathbf{D}^{\mathrm{e}}\, \dot{\boldsymbol{\varepsilon}} - (h + \mathbf{n}^{\mathrm{T}} \mathbf{D}^{\mathrm{e}}\, \mathbf{n}) \dot{\lambda} + g_{\eta} \nabla^{2} \dot{\lambda} \right] \mathrm{d}\Omega = - \int_{\Omega} \delta\lambda\, f\left(\boldsymbol{\sigma}^{t}, \kappa^{t}, \nabla^{2} \kappa^{t} \right) \mathrm{d}\Omega \qquad [15]$$

in which the following relations are considered

$$\boldsymbol{\sigma}^{t+\Delta t} = \boldsymbol{\sigma}^{t} + \int_{t}^{t+\Delta t} \dot{\boldsymbol{\sigma}}\, \mathrm{d}\tau$$

$$f\left(\boldsymbol{\sigma}^{t+\Delta t}, \kappa^{t+\Delta t}, \nabla^{2} \kappa^{t+\Delta t} \right) = f\left(\boldsymbol{\sigma}^{t}, \kappa^{t}, \nabla^{2} \kappa^{t} \right) + \int_{t}^{t+\Delta t} \dot{f}\, \mathrm{d}\tau \qquad [16]$$

The gradient to the yield surface $\mathbf{n}$ which indicates the plastic flow direction, the softening modulus h and the additional variable g_{η} are given as follows,

$$\mathbf{n} = \frac{\partial f}{\partial \boldsymbol{\sigma}} = \frac{\partial \tau(\boldsymbol{\sigma})}{\partial \boldsymbol{\sigma}}$$

$$h\left(\kappa, \nabla^{2} \kappa \right) = - \frac{\dot{\kappa}}{\dot{\lambda}} \frac{\partial f}{\partial \kappa} = \eta \frac{\partial \bar{\tau}_{\mathrm{g}}}{\partial \kappa} \qquad [17]$$

$$g_{\eta}(\kappa, l) = \eta \frac{\partial f}{\partial \nabla^{2} \kappa} = \eta \frac{\partial \bar{\tau}_{\mathrm{g}}}{\partial \nabla^{2} \kappa} = \eta\, g(\kappa, l)$$

They are determined for $\left(\boldsymbol{\sigma}^{t}, \kappa^{t}, \nabla^{2} \kappa^{t} \right)$. It is emphasized that for $g_{\eta} = 0$ the classical local plasticity equations are found.

Application of Green's theorem to the last term on the left hand side of Eq.(15) yields the non-standard boundary conditions that the plastic multiplier field must fulfill on the boundary that separates the elastic and plastic domains :

$$\delta\dot{\lambda} = 0 \quad \text{or} \quad (\nabla \dot{\lambda})^{\mathrm{T}} \mathbf{v}_{\lambda} = 0 . \qquad [18]$$

with ν_λ the outward normal at this boundary. These extra-boundary conditions should be considered as natural boundary conditions of the Cauchy problem governing the plastic flow. They should be enforced analytically to reproduce the observed physics, nor plastic strain $(18)_1$ on the external boundary far from the localization zone nor its flux $(18)_2$ through symmetry and body boundary. From the numerical point of view, the use of C^1 continuous shape functions for the interpolation of the plastic multiplier field will allow us to introduce explicitly these conditions on the external boundary of the body in order to avoid zero energy modes on the plastic field.

3. Finite element and time discretizations

The displacement, acceleration and strain fields in Eqs.(14) and (15) can be discretized according to the classical finite element procedure

$$\mathbf{u} = \mathbf{N}\mathbf{a}\,,\ \ddot{\mathbf{u}} = \mathbf{N}\ddot{\mathbf{a}}\,,\ \boldsymbol{\varepsilon} = \mathbf{B}\mathbf{a} \qquad [19]$$

where $\mathbf{N}$ contains interpolation polynomials and $\mathbf{B} = \mathbf{L}\mathbf{N}$. The vectors $\mathbf{a}$ and $\ddot{\mathbf{a}}$ are the nodal displacement and acceleration vectors, respectively. For the interpolation of the plastic multiplier that satisfies the weak form of the consistency condition (15), we introduce a vector of nodal values Λ that gives

$$\lambda = \mathbf{H}^{\mathrm{T}}\Lambda \quad,\quad \nabla^2\lambda = \mathbf{P}^{\mathrm{T}}\Lambda \qquad [20]$$

where $\mathbf{H} = [H_1,...,H_n]^T$ and $\mathbf{P} = \left[\nabla^2 H_1,...,\nabla^2 H_n\right]^T$.

Substituting the above identities in Eqs.(14) and (15) and requiring that these equations hold for any admissible variation $\delta\mathbf{a}$ and $\delta\Lambda$, we obtain the following set of algebraic equations

$$\begin{bmatrix} \mathbf{M}_{aa} & 0 \\ 0 & 0 \end{bmatrix} \begin{Bmatrix} \ddot{\mathbf{a}}^{t+\Delta t} \\ \Lambda^{t+\Delta t} \end{Bmatrix} + \begin{bmatrix} \mathbf{K}_{aa} & \mathbf{K}_{a\ddot{e}} \\ \mathbf{K}_{\ddot{e}a} & \mathbf{K}_{\ddot{e}\ddot{e}} \end{bmatrix} \begin{Bmatrix} \ddot{\mathbf{a}} \\ \ddot{\Lambda} \end{Bmatrix} = \begin{Bmatrix} \mathbf{f}_e^{\,t+\Delta t} - \mathbf{f}_i^{\,t} \\ \mathbf{f}_{\ddot{e}}^{\,t} \end{Bmatrix} \qquad [21]$$

with the elastic stiffness matrix $\mathbf{K}_{aa}$, the mass matrix $\mathbf{M}_{aa}$, the external force vector $\mathbf{f}_e$ and the internal force vector $\mathbf{f}_i$ defined conventionally, and the off-diagonal matrix $\mathbf{K}_{\lambda a}$ and the gradient dependent matrix $\mathbf{K}_{\lambda\lambda}$ defined as

$$\mathbf{K}_{a\ddot{e}} = -\int_\Omega \mathbf{H}\mathbf{n}_j^{\mathrm{T}}\mathbf{D}\mathbf{B}\mathrm{d}\Omega \ ,\ \mathbf{K}_{\lambda\lambda} = \int_\Omega \left[\left(h + \mathbf{n}_j^{\mathrm{T}}\mathbf{D}\mathbf{n}_j\right)\mathbf{H}\mathbf{H}^{\mathrm{T}} - g_\varsigma \mathbf{H}\mathbf{P}^{\mathrm{T}}\right]\mathrm{d}\Omega\,. \qquad [22]$$

Concerning the extra-boundary conditions, Green's theorem has not been applied in this approach to the last term of the left hand side of Eq.(15) and therefore the

second gradient of the shape functions $\mathbf{P}$ used for the interpolation of the plastic multiplier field appears in the sub-stiffness operator given by Eq.(22-right). As a consequence, the extra-boundary conditions are not needed to avoid zero energy modes related to the second field in this mixed formulation. However, a reduced integration is used here for avoiding numerical oscillations in the yield function, such that zero energy modes (corresponding to the number of lacking integration points) rise [HUG°87]. To overcome this issue, extra-boundary conditions are imposed on the external boundary of the body (for numerical purpose only) since C^1 continous shape function for the plastic multiplier is used.

The vector of non-standard residual forces $\mathbf{f}_\lambda$, which emerge from the inexact fulfillment of the yield condition (3) during equilibrium iteration *j*, reads

$$\mathbf{f}_\lambda = \int_\Omega f\left(\sigma_j, \kappa_j, \nabla^2 \kappa_j\right) \mathbf{H}\, d\Omega \qquad [23]$$

and the increments of nodal displacements $\ddot{A}\mathbf{a}$ and of nodal values of plastic multiplier field $\ddot{A}\Lambda$ are given by

$$\begin{aligned} \Delta\mathbf{a} &= \mathbf{a}^{t+\ddot{A}t} - \mathbf{a}^t = \int_t^{t+\ddot{A}t} \dot{\mathbf{a}}\, d\tau \\ \Delta\Lambda &= \Lambda^{t+\ddot{A}t} - \Lambda^t = \int_t^{t+\ddot{A}t} \dot{\Lambda}\, d\tau \end{aligned} \qquad [24]$$

Note that the tangent stiffness matrix in the set (21) is non-symmetric due to gradient terms in the submatrix $\mathbf{K}_{\lambda\lambda}$.

The above set of equations governs the element behavior during plastic flow. However, according to Kuhn-Tucker conditions,

$$\dot{\lambda} \geq 0 \ , \ f \leq 0 \ , \ \dot{\lambda} f = 0, \qquad [25]$$

Eqs.(21)-(23) can be extended to the elastic part of the body. In the elastic elements we set the gradient vector $\mathbf{n} = 0$ and therefore $\mathbf{K}_{\lambda a} = 0$, even this gradient is non-zero. Then the second equation in the set (21) separates from the first one giving the following equation in $d\Lambda$

$$\mathbf{K}_{\lambda\lambda} d\Lambda = \mathbf{f}_\lambda . \qquad [26]$$

For the elastic state we also set the residual forces $\mathbf{f}_\lambda$ to zero. We then obtain the desired solution $d\Lambda = \mathbf{0}$ (which satisfies the Kuhn-Tucker conditions) if the global matrix $\mathbf{K}_{\lambda\lambda}$ is non singular after element assembly and introduction of the

1	Compute constants : $c_0 = \frac{1}{\beta \Ä t^2}$, $c_1 = \frac{1}{\beta \Ä t}$, $c_2 = \frac{1}{2\beta} - 1$, $c_3 = (1-\gamma)\Ä t$, $c_4 = \gamma \Ä t$
2	Initialize : $\mathbf{a}^t, \dot{\mathbf{a}}^t, \ddot{\mathbf{a}}^t$
3	Evaluate : $\hat{\mathbf{K}}^t = \overline{\mathbf{K}}^t + c_0 \overline{\mathbf{M}}$, $\hat{\mathbf{f}}^{t+\Ä t} = \mathbf{f}_e^{t+\Ä t} + \mathbf{M}_{aa}\left(c_1 \dot{\mathbf{a}}^t + c_2 \ddot{\mathbf{a}}^t\right) - \mathbf{f}_i^t$
4	Solve for displacement and plastic multiplier increments : $\hat{\mathbf{K}}^t \begin{Bmatrix} \Ä \mathbf{a} \\ \Ä \Lambda \end{Bmatrix} = \begin{Bmatrix} \hat{\mathbf{f}}^{t+\Ä t} \\ \mathbf{f}_\lambda^t \end{Bmatrix}$
5	Equilibrium iterations : j=1 $^{(0)}\Ä \mathbf{a} = \Ä \mathbf{a}$, $^{(0)}\Ä \Lambda = \Ä \Lambda$ $^{(j-1)}\ddot{\mathbf{a}}^{t+\Delta t} = c_0\, {}^{(j-1)}\Ä \mathbf{a} - c_1 \dot{\mathbf{a}}^t - c_2 \ddot{\mathbf{a}}^t$ $^{(j-1)}\hat{\mathbf{K}} = {}^{(j-1)}\overline{\mathbf{K}}^{t+\Ä t} + c_0 \overline{\mathbf{M}}$ $^{(j)}\hat{\mathbf{f}} = \mathbf{f}_e^{t+\Ä t} - \mathbf{M}_{aa}\, {}^{(j-1)}\ddot{\mathbf{a}}^{t+\Ä t} - {}^{(j-1)}\mathbf{f}_i^{t+\Ä t}$ $^{(j-1)}\mathbf{f}_\lambda^{t+\Ä t}$
6	Solve for delta-increments : $^{(j-1)}\hat{\mathbf{K}}^{t+\Ä t} \begin{Bmatrix} \Ä \Ä \mathbf{a} \\ \Ä \Ä \Lambda \end{Bmatrix} = \begin{Bmatrix} {}^{(j)}\hat{\mathbf{f}}^{t+\Ä t} \\ {}^{(j-1)}\mathbf{f}_\lambda^{t+\Ä t} \end{Bmatrix}$
7	Evaluate : $^{(j)}\Ä \mathbf{a} = {}^{(j-1)}\Ä \mathbf{a} + {}^{(j)}\Ä \Ä \mathbf{a}$, $^{(j)}\Ä \Lambda = {}^{(j-1)}\Ä \Lambda + {}^{(j)}\Ä \Ä \Lambda$
8	Check convergence criterion : If non-converged $j = j+1$ go to 5.
9	Calculate new accelerations, velocities and displacements : $\ddot{\mathbf{a}}^{t+\Ä t} = c_0 \Ä \mathbf{a} - c_1 \dot{\mathbf{a}}^t - c_2 \ddot{\mathbf{a}}^t$ $\dot{\mathbf{a}}^{t+\Ä t} = \dot{\mathbf{a}}^t + c_3 \ddot{\mathbf{a}}^t + c_4 \ddot{\mathbf{a}}^{t+\Ä t}$ $\mathbf{a}^{t+\Ä t} = \mathbf{a}^t + \Ä \mathbf{a}$
10	Next time step, go to 3.

Figure 1. *Algorithm for Newmark time integration schema used in a Newton-Raphson iterative procedure*

boundary conditions for the Λ degrees-of-freedom [PAM°94]. Moreover, the elastic predictor plastic corrector algorithm allows us to distinguish the plastic domain from the elastic one where the penalization should occur.

Equation (21) represents the semi-discrete nonlinear equation of motion governing the response of the discretized continuum. A direct time integration method is needed to obtain the full-discrete equation of motion.

In the above derivation we have tacitly considered that the equation of motion is satisfied at time $t+\Delta t$ which corresponds to an implicit time integration of field equations. An explicit time integration schema could also be considered, where the motion equation is assumed to be satisfied at time t. The explicit schema allows us to reduce the computational time since no equilibrium iterations within the time step are required. Furthermore, it needs neither factorization nor storage of the stiffness matrix. However, for the gradient plasticity model, equilibrium iterations are required within the time step. Indeed, since non-standard residual forces $\mathbf{f}_\lambda$ emerge from the inexact fulfillment of the yield condition, these iterations will allow the stress state to become plastically admissible only at the end of the time step. Therefore, the Newmark implicit schema is retained. The main assumption is that the acceleration varies linearly over the time step. The algorithm for the Newmark integration schema used in the Newton-Raphson iterative procedure is outlined in the box of Fig.1, where

$$\overline{\mathbf{M}} = \begin{bmatrix} \mathbf{M}_{aa} & 0 \\ 0 & 0 \end{bmatrix}, \quad \overline{\mathbf{K}}^t = \begin{bmatrix} \mathbf{K}_{aa} & \mathbf{K}_{a\lambda} \\ \mathbf{K}_{\lambda a} & \mathbf{K}_{\lambda\lambda} \end{bmatrix} \qquad [27]$$

and the coefficients β and γ should satisfy the following conditions

$$\gamma \geq \frac{1}{2} \text{ and } \beta \geq \frac{1}{4}\left(\gamma + \frac{1}{2}\right)^2 \qquad [28]$$

in order to ensure stability of the algorithm in linear analyses [BAT°82]. For the wave propagation analysis presented in this paper, the prominent constant or average acceleration method is used, which is obtained by setting $\beta = 1/4$ and $\gamma = 1/2$.

4. Layered finite element formulation

4.1. *Discretization principle*

Structural behavior of beams may be satisfactorily approximated by the elementary Euler-Bernoulli theory of bending. The main assumption in this theory is that the transverse normal to the reference middle plane remains so during bending, implying that the transverse shear strain becomes zero. Thus, the bending rotation

becomes a first derivative of transverse displacement v and hence the theory requires the transverse displacement field to be C^1 continuous. Therefore, the stress and strain tensors reduce to their axial components $\sigma = [\sigma]^T$ and $\varepsilon = [\varepsilon]^T$, respectively and the Hooke matrix reads $\mathbf{D}^e = [\mathrm{E}]$, E is the Young modulus [2].

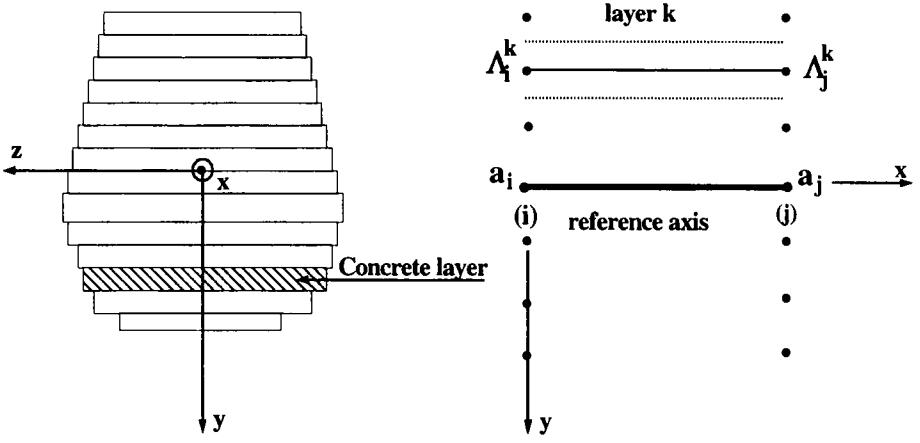

Figure 2. *Multilayered finite element discretization*

The Euler-Bernoulli assumption allows us to relate the displacement and the strain in any point of the cross section of the beam (Fig.2) to the displacement of the reference axis as follows

$$\mathbf{u} = \begin{vmatrix} u(x,y) = u(x,0) - y\dfrac{\partial v(x,0)}{\partial x} \\ v(x,y) = v(x,0) \end{vmatrix} \quad , \quad \varepsilon = \begin{vmatrix} \varepsilon(x,y) = \varepsilon_{xx} = \dfrac{\partial u(x,y)}{\partial x} = u_{,x} - y\ v_{,xx} \\ \gamma_{xy} = 2\varepsilon_{xy} = 0 \end{vmatrix} \quad [29]$$

where γ_{xy} is the shear strain. Therefore the approach consists of discretizing only the displacement corresponding to the reference axis of the beam finite element.

Now we focus our attention on the plastic multiplier field that should be discretized due to the weak satisfaction of the yield condition. No assumption can be made concerning its variation through the cross section. This is then divided into n superposed layers (Fig.2), representing the variation of the plastic multiplier in this direction. On each layer k, the plastic state of the point is interpolated by means of nodal parameters $\Lambda^k = \left(\Lambda_i^k, \Lambda_j^k\right)$ giving the evolution in the axial direction of the

element. The obtained beam element has a mixed character and presents a variable number of d-o-f

$$\mathbf{a}_g = \left(\mathbf{a}, \Lambda^1, ..., \Lambda^k, ..., \Lambda^n\right) \qquad [30]$$

where n is the number of the layers and $\mathbf{a}_g$ is a vector gathering the nodal values of both the displacement and the plastic multiplier fields. The vectors $\mathbf{a}$ and Λ^k are specified in the next section for the proposed element.

We proceed in the same way as in the previous section by considering, on the one hand, the above discretizations (Eq.30), and on the other, the two variational equations (14) and (15). We then obtain the algebraic equations,

$$\begin{bmatrix} [\mathbf{M}_{aa}] & [\mathbf{0}] & \cdots & [\mathbf{0}] & \cdots & [\mathbf{0}] \\ [\mathbf{0}] & [\mathbf{0}] & \cdots & [\mathbf{0}] & \cdots & [\mathbf{0}] \\ \vdots & \vdots & \ddots & \vdots & \ddots & \vdots \\ [\mathbf{0}] & [\mathbf{0}] & \cdots & [\mathbf{0}] & \cdots & [\mathbf{0}] \\ \vdots & \vdots & \ddots & \vdots & \ddots & \vdots \\ [\mathbf{0}] & [\mathbf{0}] & \cdots & [\mathbf{0}] & \cdots & [\mathbf{0}] \end{bmatrix} \begin{bmatrix} \ddot{\mathbf{a}}^{t+\ddot{A}t} \\ {}^1\ddot{\Lambda}^{t+\ddot{A}t} \\ \vdots \\ {}^k\ddot{\Lambda}^{t+\ddot{A}t} \\ \vdots \\ {}^n\ddot{\Lambda}^{t+\ddot{A}t} \end{bmatrix} +$$

$$\begin{bmatrix} [\mathbf{K}_{aa}] & [\mathbf{K}^1_{\lambda a}]^T & \cdots & [\mathbf{K}^k_{\lambda a}]^T & \cdots & [\mathbf{K}^n_{\lambda a}]^T \\ [\mathbf{K}^1_{\lambda a}] & [\mathbf{K}^1_{\lambda\lambda}] & \cdots & [\mathbf{0}] & \cdots & [\mathbf{0}] \\ \vdots & \vdots & \ddots & \vdots & \ddots & \vdots \\ [\mathbf{K}^k_{\lambda a}] & [\mathbf{0}] & \cdots & [\mathbf{K}^k_{\lambda\lambda}] & \cdots & [\mathbf{0}] \\ \vdots & \vdots & \ddots & \vdots & \ddots & \vdots \\ [\mathbf{K}^n_{\lambda a}] & [\mathbf{0}] & \cdots & [\mathbf{0}] & \cdots & [\mathbf{K}^n_{\lambda\lambda}] \end{bmatrix} \begin{bmatrix} \ddot{A}\mathbf{a} \\ \ddot{A}\Lambda^1 \\ \vdots \\ \ddot{A}\Lambda^k \\ \vdots \\ \ddot{A}\Lambda^n \end{bmatrix} = \begin{bmatrix} \mathbf{f}_e^{t+\ddot{A}t} - \mathbf{f}_i^t \\ {}^1\mathbf{f}_\lambda^t \\ \vdots \\ {}^k\mathbf{f}_\lambda^t \\ \vdots \\ {}^n\mathbf{f}_\lambda^t \end{bmatrix} \qquad [31]$$

in compact fashion, to solve for the layered beam element in gradient plasticity where the coupling matrix $[\mathbf{K}^k_{\lambda a}]$, the gradient-dependent matrix $[\mathbf{K}^k_{\lambda\lambda}]$ and the non-standard residual forces $\mathbf{f}^k_\lambda$ are defined in Eqs.(22)-(23) and the subscript k indicates that quantities are computed with respect to the considered layer.

4.2. *Interpolation of the fields*

The interpolation of the displacement field at the mid-axis of the beam is given by

$$\mathbf{u} = \mathbf{N}\,\mathbf{a} = \begin{bmatrix} \mathbf{N}^u \\ \mathbf{N}^v \end{bmatrix} \begin{Bmatrix} \mathbf{a}^u \\ \mathbf{a}^v \end{Bmatrix} \qquad [32]$$

where $\mathbf{N}^u$ and $\mathbf{N}^v$ are the shape functions corresponding to components u et v, respectively. A quadratic interpolation of u is adopted in order to ensure compatibility between the two fields due to the mixed character of the formulation. Furthermore, Eq.(29) shows the need of a cubic interpolation of the transverse component of displacement. Two degrees of freedom per node are then needed for this component (Fig.3).

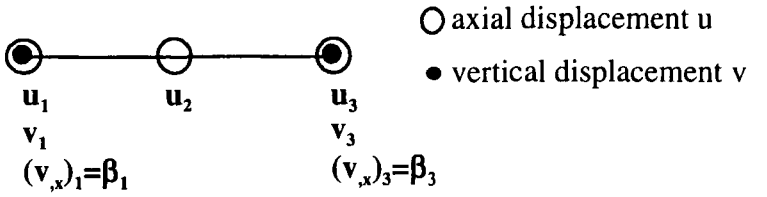

Figure 3. *Degrees of freedom of the beam*

The expressions of the shape functions appearing in relation (32) are given by

$$\left|\begin{array}{l} Node\,1:\xi_1 = -1 \\ N_1^u(\xi) = \dfrac{\xi(\xi-1)}{2} \\ N_1^v(\xi) = \dfrac{1}{4}(1-\xi)^2(2+\xi) \\ N_2^v(\xi) = \dfrac{l_e}{8}(1-\xi^2)(1-\xi) \end{array}\right. ; \left|\begin{array}{l} Node\,2:\xi_2 = 0 \\ N_2^u(\xi) = 1-\xi^2 \end{array}\right. ; \left|\begin{array}{l} Node\,3:\xi_3 = 1 \\ N_3^u(\xi) = \dfrac{\xi(\xi+1)}{2} \\ N_3^v(\xi) = \dfrac{1}{4}(1+\xi)^2(2-\xi) \\ N_4^v(\xi) = \dfrac{-l_e}{8}(1-\xi^2)(1+\xi) \end{array}\right. \qquad [33]$$

where the passage from the local to the Cartesian coordinates is given by $\xi = 2x/l_e - 1$ and $\eta = 2y/h_e$; l_e is the length of the element and h_e its height. The nodal displacement vector **a** and the matrix **B** read

$$\mathbf{a}^T = \left[u_1 \quad u_2 \quad u_3 \quad v_1 \quad \beta_1 = (v_{,x})_1 \quad v_3 \quad \beta_3 = (v_{,x})_3\right] \qquad [34]$$

and

$$\mathbf{B}=\left[\left(\frac{4x}{l_e^2}-\frac{3}{l_e}\right)\ \left(\frac{-8x}{l^2}-\frac{4}{l_e}\right)\ \left(\frac{4x}{l_e^2}-\frac{1}{l_e}\right)\ y\left(\frac{6}{l_e^2}-\frac{12x}{l_e^3}\right)\right.$$
$$\left. y\left(\frac{4}{l_e}-\frac{6x}{l_e^2}\right)\ y\left(\frac{12x}{l_e^3}-\frac{6}{l_e^2}\right)\ y\left(\frac{2}{l_e}-\frac{6x}{l_e^2}\right)\right]. \qquad [35]$$

The elastic stiffness matrix and the internal forces vector appearing in the relation (31) can be expressed as follows

$$\mathbf{K}_{aa}=b_e\,\mathrm{E}\int_0^{l_e}\int_{-h_e/2}^{+h_e/2}\mathbf{B}^{\mathrm{T}}(x,y)\mathbf{B}(x,y)\,\mathrm{d}y\,\mathrm{d}x$$
$$\mathbf{f}_i=b_e\int_0^{l_e}\int_{-h_e/2}^{+h_e/2}\sigma(x,y)\mathbf{B}^{\mathrm{T}}(x,y)\,\mathrm{d}y\,\mathrm{d}x \qquad [36]$$

where b_e is the width of the beam element (rectangular beams are considered). Note that the quantity β of the nodal displacement vector (Eq.34) represents the rotation of the cross section.

Concerning the interpolation of the plastic multiplier field, it is necessary to use C^1 continuous shape functions since second derivatives of this variable appear in both of the definition of the gradient dependent matrix $\mathbf{K}_{\lambda\lambda}$ and the non-standard residual forces vector $\mathbf{f}_\lambda$. The same shape functions as for the transverse displacement are used, i.e. $\mathbf{H}^\lambda=\mathbf{N}^v$. Therefore, at any point of each layer k (Fig.4), the plastic multiplier is interpolated using two degrees of freedom per node; the nodal value of λ^k and its first derivative. The vector of the nodal parameters ${}^k\Lambda$ is then given by

$${}^k\Lambda=\left(\Lambda_1^k,\Lambda_3^k\right)=\left({}^k\ddot{\mathrm{E}}^1,\ {}^k\ddot{\mathrm{E}}^1_{,x},\ {}^k\ddot{\mathrm{E}}^3,\ {}^k\ddot{\mathrm{E}}^3_{,x},\right) \qquad [37]$$

and the different matrices appearing in eq. (31) and defined by the relation (22) are given as follows

$${}^k\mathbf{K}_{a\lambda}=-\,\mathrm{b_e}\,\mathrm{E}\int_0^{l_e}\int_{y_k-e_k/2}^{y_k+e_k/2}\mathbf{B}^{\mathrm{T}}(x,y)\ {}^k\mathbf{n}(x,y)\mathbf{H}^\lambda(x)\,\mathrm{d}y\,\mathrm{d}x \qquad [38]$$

$${}^k\mathbf{K}_{\lambda\lambda}=-\ {}^k\mathrm{S}\int_0^{l_e}\left[(h+\mathrm{E})\mathbf{H}^\lambda(x)\mathbf{H}^{\lambda\,\mathrm{T}}(x)+g\,\mathbf{H}^\lambda(x)\mathbf{P}^{\mathrm{T}}(x)\right]\mathrm{d}x \qquad [39]$$

where the non-symmetric definition of $\mathbf{K}_{\lambda\lambda}$ is considered with e_k the thickness of the layer, ${}^k\mathrm{S}$ its cross section and y_k the distance from the reference axis (Fig.4).

Furthermore, the non-standard residual forces vector is

$$ {}^k\mathbf{f}_\lambda = {}^kS \int_0^{l_e} f\left(\sigma(x, y_k), {}^k\lambda(x), {}^k\lambda_{,xx}(x)\right)\mathbf{H}^\lambda(x)\,\mathrm{d}x \qquad [40] $$

in which the plastic multiplier ${}^k\lambda(x)$ is computed from the corresponding nodal values on the concerned layer ${}^k\Lambda$ and the stress state is obtained such $\sigma(x, y_k) = \sigma^t(x, y_k) - \mathrm{E}\,\mathrm{d}\lambda^k(x)\left.\frac{\partial f}{\partial \sigma}\right|_{\sigma^t}$ where $\sigma^\tau = \sigma_0 + \mathrm{E}\,\mathbf{B}(x, y_k)\,\mathbf{da}$ is the trial stress state and σ_0 is the stress of the previous step.

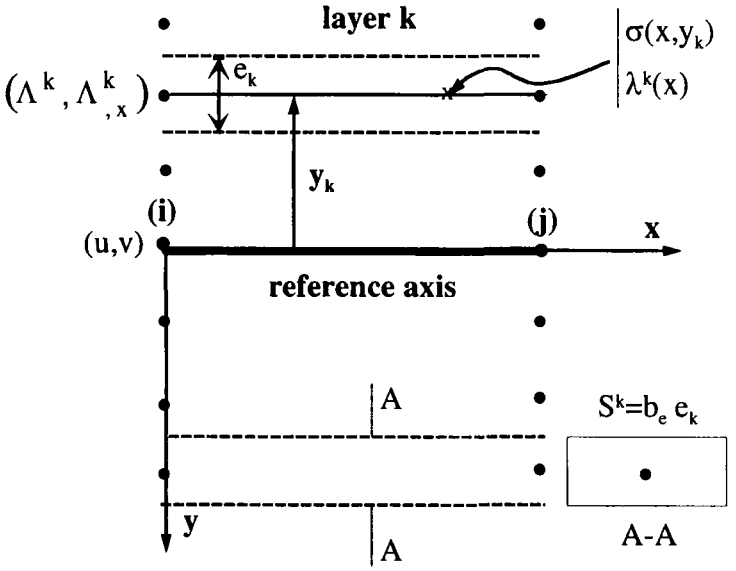

Figure 4. *Elastoplastic state of a point located on a layer k*

A variational principle for associated gradient plasticity has been proposed in [MUH°91], which results in the symmetric definition of the sub-matrix $\mathbf{K}_{\lambda\lambda}$ and suggests the use of $\overset{0}{\mathrm{C}}$ continuous elements in terms of plastic multiplier interpolation. However, it is not sufficient to make the tangent stiffness operator

symmetric to reduce the continuity requirements: the non-standard residual terms $\mathbf{f}_\lambda$ must also be reformulated. Furthermore, the additional boundary condition $(18)_2$ calls for the existence of first derivatives of λ as nodal degrees-of-freedom. Another approach consists in a weak satisfaction of the consistency condition instead of the yield function. In this case, the residual forces $\mathbf{f}_\lambda$ will not appear in the right hand side of the relation (31). This means that the stress state will not be mapped to the yield surface during the first iteration of a current step. In our approach however, the forces $\mathbf{f}_\lambda$ should appear in order to ensure and control propagation of plasticity between the layers. The evolution of plasticity in the height direction is then made possible only when the yield criterion is violated by the stress state on layers. Therefore, non-zero values of $\mathbf{f}_\lambda$ corresponding to the concerned layers appear in the solved set of equations (31). It becomes clear that the nodal parameters ${}^k\Lambda$ are not completely independent, but that they are coupled with the kinematic of the element by means of the non-standard residual forces whose values depend on a stress state $\sigma(x, y)$. Finally, it is emphasized that no convergence of the iterative procedure has been observed when only a weak satisfaction of the consistency condition is considered [MEF°95]. Furthermore, the symmetrization does not seem to offer much practical advantage, it rather results in numerical troubles [MEF°95].

5. Material model

Since we restrict the analysis to Euler-Bernoulli beam theory, the layers present one dimensional plastic flow. Therefore a second order gradient yield function can be summarized by the following equation

$$f(\sigma, \bar{\tau}_g) = \sigma - \bar{\tau}_g(\varepsilon^p, \varepsilon^p_{,xx}) = \sigma - \bar{\tau}(\varepsilon^p) - g(\varepsilon^p)\frac{\mathrm{d}^2\varepsilon^p}{\mathrm{d}x^2} \qquad [41]$$

with $\varepsilon^p \equiv \lambda \equiv \kappa$ when a uniaxial yield function is considered. This definition of the gradient yield function is valid for the behavior of concrete in both tension and compression. The main difference consists in the definition of the local (classical) yield function $\bar{\tau}$ which differs from tension to compression. The same plastic strain field is then used for both the tension and compression.

In tension the Young's modulus E governs the relation between stress and strain: $\sigma = E \cdot \varepsilon$ in elastic regime. When the maximum tensile strength f_t is attained (Fig.5) softening occurs according to either a linear diagram given by

$$\bar{\tau} = f_t\left(1 - \frac{\varepsilon^p}{{}^l\varepsilon^p_u}\right) \qquad [42]$$

or a nonlinear diagram given by [HOR°91]

$$\bar{\tau} = f_t \left[\left(1 - \left(c_1 \frac{\varepsilon^p}{{}^{nl}\varepsilon_u^p} \right)^3 \right) \exp\left(-c_2 \frac{\varepsilon^p}{{}^{nl}\varepsilon_u^p} \right) - \left(1 + c_1^3 \right) \frac{\varepsilon^\pi}{{}^{nl}\varepsilon_u^p} \exp(-c_2) \right] \qquad [43]$$

where ${}^{l}\varepsilon_u^p$ and ${}^{nl}\varepsilon_u^p$ are the ultimate plastic strains and $c_1 = 3.0$ et $c_2 = 6.93$.

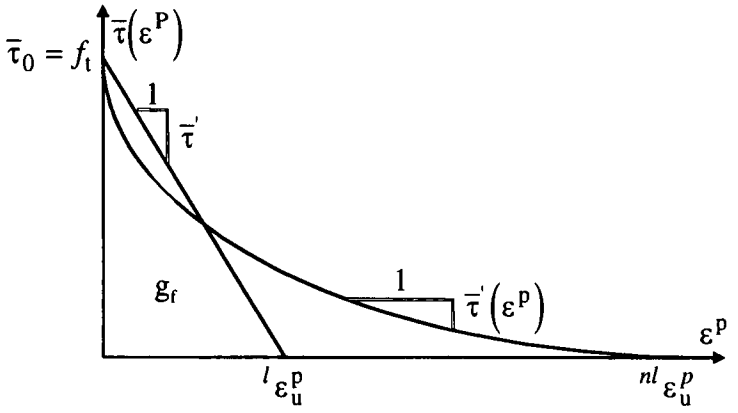

Figure 5. *Linear and nonlinear local softening diagram in gradient plasticity*

In order to define completely the local plastic flow diagram, the ultimate plastic strain should be computed. It is given for both linear and nonlinear softening diagrams such

$${}^{l}\varepsilon_u^p = 2\frac{g_f}{f_t} \quad , \quad {}^{nl}\varepsilon_u^p = 5.14\frac{g_f}{f_t} \qquad [44]$$

where g_f is the energy dissipated locally given by the area under the $\bar{\tau} - \varepsilon^p$ diagram (Fig.5). The constitutive model herein investigated follows a smeared crack approach considering the fracture energy G_f (which is the amount of energy required to open a unit crack area [HIL°76]) associated to mode I failure as a material parameter. Although this energy can be strongly affected by the interaction with mode II, as pointed out by [ROT°87], mode I usually prevails in concrete structures. This assumption, experimentally validated by various authors [NOO°92], justifies the need to describe carefully this failure mode fixing some key-parameters, which control its evolution in boundary value problems. A characteristic length h is

then introduced in the model making it possible to get link between the fracture energy G_f and the energy dissipated locally g_f (at the material point level) [BAZ°83a, BAZ°83b] :

$$g_f = \frac{G_f}{h} \qquad [45]$$

For this gradient model, the fracture energy is considered to be dissipated over a zone that represents the localization band (Fig.6) whose size w is given analytically [BOR°92] as

$$w = 2\pi l \qquad [46]$$

where l is an internal length parameter appearing in the model due to the nonlocal character of the theory. This parameter governs the effective contribution of the gradient term in Eq.(41) through the weight function g such

$$g\left(\varepsilon^p, l\right) = -l^2\, \bar{\tau}'\left(\varepsilon^p\right) \qquad [47]$$

where $\bar{\tau}'$ is the slope of the softening diagram. If this weight function is zero the classical formulation is retrieved. It is assumed that for nonlinear softening the gradient influence on the nonlocal limit stress $\bar{\tau}$ decreases with the increase of the cumulated inelastic strain κ, which in reality represents the crack opening. However, a small value of the variable g is kept to maintain gradient effects when ε^p exceeds the ultimate strain (since in this case $\bar{\tau}'\left(\varepsilon^p\right) = 0$).

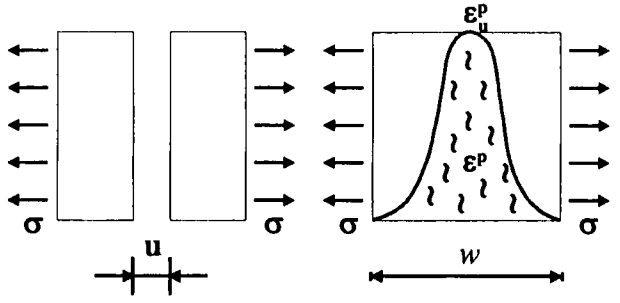

Figure 6. *Discrete crack concept (left) and plastic strain variation in the localization zone for a nonlocal smeared crack approach (right)*

Furthermore, it is emphasized that the presence of gradient terms in the yield strength is the algorithmic essence of gradient regularization. The case of a negative contribution of this term occurs on the elastoplastic boundary, making possible the spreading of the localization zone due to the fact that the nonlocal yield strength $\bar{\tau}_g$

reduces (Eq.41). Moreover, while severe gradient effects may occur in the transverse direction during loading, they are not taken into account in the considered model. The plasticity propagates between layers only due to the violation of the yield function by the stress state; gradient regularization acts only in the axial direction.

According to Eqs.(42)-(46)

$$G_f = \int \sigma \, du = \int \left(\int \sigma \, d\varepsilon^p \right) dw = (\alpha \cdot w) \cdot g_f = h \cdot g_f \qquad [48]$$

an analytical relation between the characteristic length h and the internal length parameter l $(w = 2\pi l)$ can then be derived

$$h = \alpha \cdot w \qquad [49]$$

in which the coefficient α appears from the integration and depends on both the profile of the plastic strain within the localization zone (it has a cosine shape Fig.6) and the softening diagram (linear or nonlinear) as shown in [MEF°97]. If the strains are assumed constant and a linear softening is considered then $\alpha = 1$. In the following the default value for α will be set equal to 2 [BOR°96]. The fracture energy can then be properly used as a material parameter to define completely the local softening diagram.

The characteristic length h has been the object of several experimental investigations [BAZ°89, FOK°92, FOK°93, PRI°97], but the results are characterized by a large scattering, even if they are always expressed in terms of the maximum aggregate size d_a $(h = 0.5 \rightarrow 7\, d_a)$. The identification of this length has also been attempted recently by means of an inverse process carried out on size effect test data [BAZ°97], or taking into account crack spacing in RC structures with a large amount of reinforcement [SLU°96]. Furthermore, in an initial boundary value problem, the characteristic length cannot be assumed to be too large compared to the geometry of the singularity, *i.e.*, the notch width or the heterogeneity dimension, because otherwise the stress intensity factor can be drastically reduced. Last, but not least, it is interesting to remember that the presence of the internal length parameter in the nonlocal models enables a meaningful simulation of the (deterministic) size effect observed in quasi brittle fracture experiments [SAO°92].

In compression a nonlinear behavior (Fig.7) can be considered locally. The local yield strength $\bar{\tau}$ is then given by the following relations [FEE°93]

$$\bar{\tau} = \frac{f_c}{3} \left(1 + 4 \frac{\varepsilon^p}{\varepsilon^p_{pic}} - 2 \frac{\left(\varepsilon^p\right)^2}{\left(\varepsilon^p_{pic}\right)^2} \right), \qquad [50]$$

before the peak of stress and

$$\bar{\tau} = f_c \left(1 - \frac{\left(\varepsilon^p - \varepsilon^p_{pic}\right)^2}{\left(\varepsilon^p_u - \varepsilon^p_{pic}\right)^2} \right) \qquad [51]$$

in the softening regime. In a similar manner as in tension, the compressive fracture energy G_c could be used as a material parameter to determine completely the local flow diagram in compression [FEE°93]. *Note that in this multilayered approach, there is no need to introduce a second discretized plastic strain field related to compressive behavior as shall be the case for a full two dimensional plain stress/strain configuration analysis.*

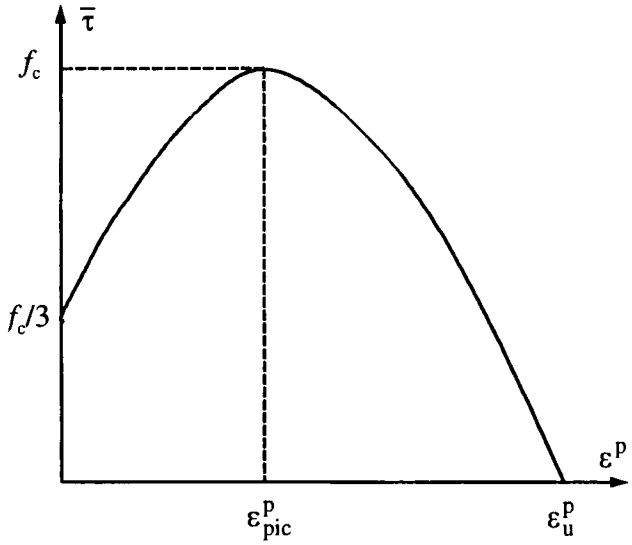

Figure 7. *Diagram of the local flow in compression*

6. Validation

The elaborated model is applied to Mode-I concrete fracture problems. Several configurations have been analyzed in static and the results compared with experimental findings and results of some other models [MEF°98]. Here, the illustration of the approach is made for problems of stress waves propagation in reinforced concrete structures. In these calculations the consistent tangent operator is employed in full Newton-Raphson scheme.

Steel fiber reinforced beam under impact

The aim of the study is to scrutinize the numerical solution when gradient regularization is used with respect to a solution that is obtained with a local model. The impact tests on the steel fiber reinforced concrete beams have been carried out at the Institute für Massivbau und Baustofftechnologie of Karlsruhe University [EIB°93]. A test result with WIREX steel fiber mixture is used for a comparison with computational analysis.

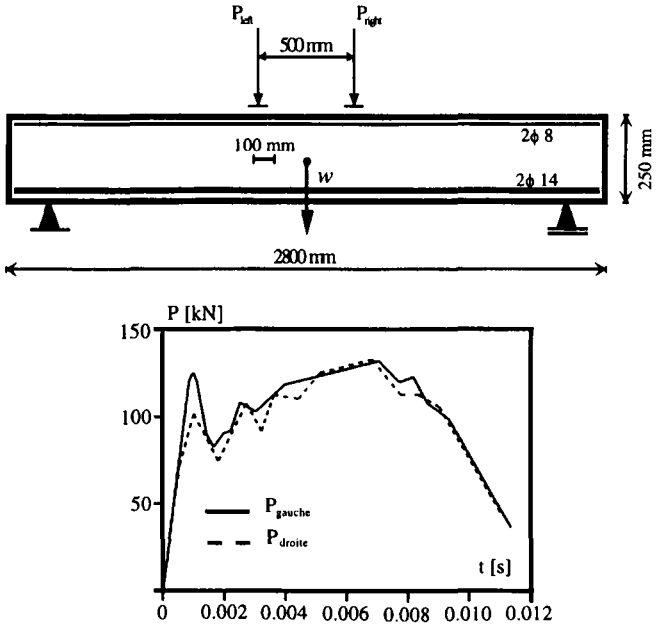

Figure 8. *Experimental set-up and load history*

The experimental set-up is shown in Fig.8. The beams have been reinforced with upper ($2\phi 8$) and lower ($2\phi 14$) steel bars. The fibers are aligned with the steel bars and are distributed randomly over the cross section of the beam. The loading is applied via two load cells in the center of the beam with a time-load characteristic given in Fig.8.

The material data are given in the table of Fig.9. For concrete, a linear softening flow is considered in tension and a nonlinear behavior is adopted in compression (see section 5). The steel bars behave in an elastoplastic manner with a slight hardening contribution after the onset of yielding. The addition of fibers to the concrete is taken into account by a phenomenological approach. Indeed, the ductility

of the cracked material is increased, and therefore a large value of the ultimate plastic strain ${}^{t}\varepsilon_u^p$ in tension (Fig.5) is considered. This large value corresponds to a greater value of the fracture energy than for plain concrete (without steel fibers). Note that the yield stresses and the Young's modulus have been taken from dynamic tests, with a strain rate $\dot{\varepsilon} = 0.038\, s^{-1}$, which is representative for the experiment.

Concrete			
E_b^{dyn}	32940	[N/mm^2]	dynamic Young modulus.
f_t^{dyn}	4.41	[N/mm^2]	dynamic tension strength.
ρ	2320	[kg/m^3]	density.
l	4 , 96	mm	internal length.
Steel bars			
E_a^{dyn}	245385	[N/mm^2]	dynamic Young modulus.
σ_e^{dyn}	638.0	[N/mm^2]	dynamic yield strength.
ρ	7800	[kg/m^3]	density.
Steel fiber			
ε_u^t	0.005		ultimate plastic/cracking strain.

Figure 9. *Material properties for the beam*

In the experiment, a bending wave is observed at an early stage ($t = 0.001\, s$) propagating from the impact points to the center of the beam (Fig.10-top). At this time, cracking first occurs below the impact zones and then propagates to the center of the beam. When the bending wave reaches the supports ($t = 0.002\, s$), the overall displacement pattern changes into a first order vibration mode (Fig.10-bottom). Therefore, the cracked zone propagates gradually in the direction of the supports until failure occurs. The diffusion of the crack zone is made possible by the steel reinforcement which enables the material to redistribute the stress as soon as cracking occurs.

Numerically, several configurations are analyzed. First, a local plasticity model is used to predict the response of the beam when no regularization technique is introduced. Then, the beam is analyzed by means of the gradient plasticity model

using two different values of the internal length $l = 4\,\text{mm}$ and $l = 96\,\text{mm}$ giving the localization zone sizes $w \approx 25\,\text{mm}$ and $w \approx 603\,\text{mm}$, respectively. It is worth noting that the characteristic length h is an input datum related to the material, like the fracture energy G_f. The value of g_f is univocally determined if G_f and h are known (Eq.45), and thus it does not depend on the finite element size. Nevertheless, in order to make the nonlocal approach successful, the finite element size must be kept lower than the internal length l, which is related to the dimension of the representative volume of the material. The selected value of the localization band width, and thus of the characteristic length h (Eq.49), is here a reasonable compromise between the specimen dimension and the used mesh since no experimental data are available from the experimental test on the maximum aggregate size [BAZ°89]. Furthermore, the scattering in the adopted values of the characteristic length is motivated by the desire to distinguish clearly how this parameter controls the crack pattern in the case of a RC structure with respect to simulations results obtained with a classical local model.

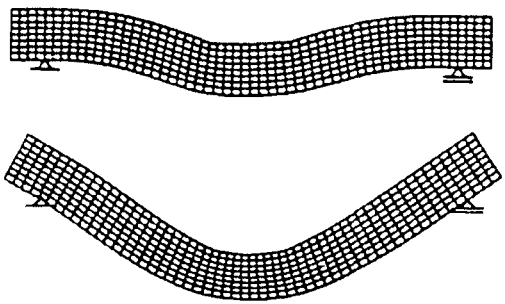

Figure 10. *Experimental deformation pattern at* $t = 0.001\,s$ *(top) and* $t = 0.002\,s$ *(bottom)*

In the local model the beam is analyzed using one coarse and one fine mesh. Figure 11 shows the coarse mesh for the gradient model using the elaborated multilayered beam finite element, where 44 elements and 9 layers are considered. Note that only the mid-axis of the beam is discretized in this multilayered approach and the layers appearing in Fig.11 correspond to the plastic multiplier evolution in the height of the beam. The steel is modeled by bar finite elements presenting an

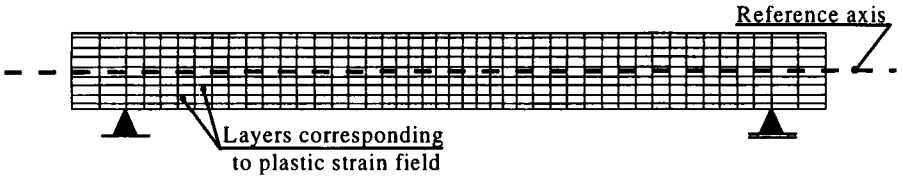

Figure 11. *Finite element mesh used for the gradient model*

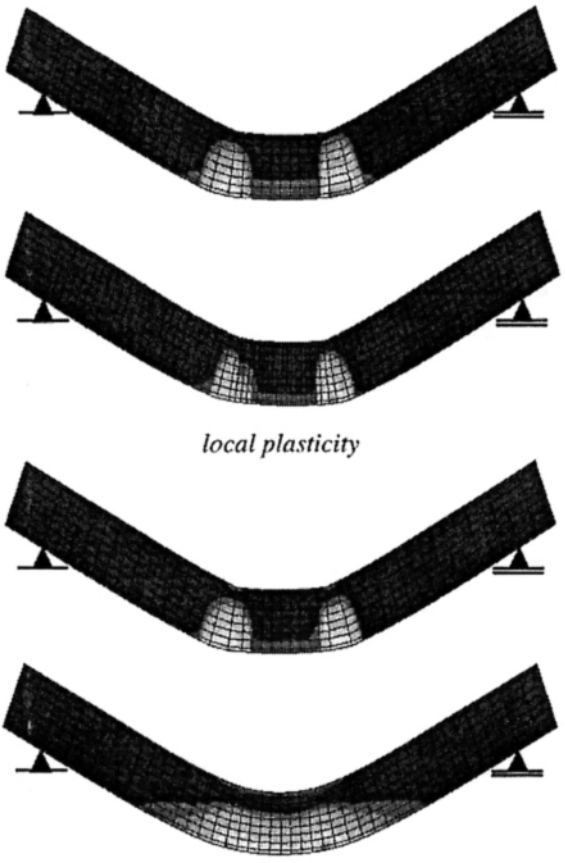

Figure 12. *Deformation and crack patterns for a local plasticity model after mesh refinement (top) and for a gradient model for two different internal lengths (bottom)*

eccentricity with respect to the mid-axis of the beam. For the interaction between the concrete and the steel bars, a perfect bond is considered. It is however recommended that in order to simulate properly the crack spacing, an interface behavior should be considered by introducing a shear traction-slip relation [SLU°95].

The differences between local and gradient plasticity models are shown in Fig.12. At a certain stage ($t = 0.004\,s$) of the analysis the yield stress in the lower reinforcement bars is exceeded. For a local plasticity model, dominant crack formation occurs in one element. Then, plastic deformation remains restricted to only one element when mesh refinement occurs (Fig.12-top), which practically precludes post-localization analysis; distributed cracking cannot be predicted and the computational analysis is very mesh sensitive.

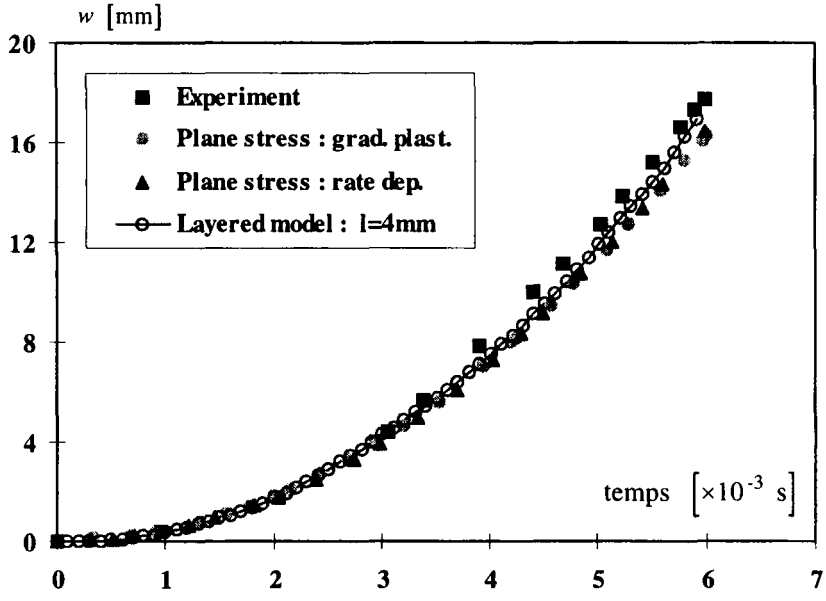

Figure 13. *Deflection-time curve for center of the beam*

For a gradient model we observe that the zone of plastic deformation spreads over a number of elements. The diffusion of the plastic deformation is governed by the internal length. Indeed, a zone of localized cracks occurs (Fig.12-bottom) when a small value of the internal length is considered instead of a zone of almost distributed deformation (Fig.12-bottom) when large value of l is introduced. An analysis with a gradient model with a very small length scale results in a similar failure mode, but without the sensitivity with respect to discretization. It is specified that small length scale effect can only be introduced in combination with fine meshes

that allow the localization zone to spread over, at least, two elements. Otherwise, the localization zone will stay confined in one element.

The uniqueness of the numerical solution has also been investigated in these meshsensitivity studies. In Fig.13, the obtained results show good agreement with experimental findings and results of some other models; a rate dependent model and a gradient model in a plane stress configuration [SLU°92b,SLU°94].

7. Conclusion

It is shown that physically meaningful results can be obtained in the post-localization regime when a gradient dependent model is used. The results of simulations show a good agreement with experiments. The internal length scale, which determines the crack band width, is related to the characteristic length which is the additional material constant that should be properly introduced. The multilayered model seems to be a promising approach which will allow us to extend the applicability of the gradient plasticity as a localization limiter. Despite the performances of the Euler model in describing Mode-I localized failures, this approach presents some drawbacks. Indeed, the Euler theory may lead to serious discrepancies in the case of deep beams with small aspects ratios where shear effects are significant. Therefore, the model should be extended in order to take into account the transverse shear stress and strain, their parabolic variation through the thickness and the warping of the cross section.

8. Bibliography

[BAT 82] Bathe K.J., *Finite element procedures in engineering analysis*, Prentice Hall, New Jerzy, 1982.

[BAT 90] Batoz J.L., Dhatt G., *Modélisation des structures par éléments finis*. Paris, Edition Hermès, vol. 2, 1990.

[BAZ 83a] BAZANT Z.P., OH B.H., « Crack band theory for fracture of concrete », Materiaux et Construction, 16(93), 155-177, (1983).

[BAZ 83b] BAZANT Z.P., CEDOLIN L., « Finite element modeling of crack band propagation », ASCE J. Struct. Engrg., 109-St2, 69-82, (1983).

[BAZ 89] BAZANT Z.P., PIJAUDIER-CABOT G., « Measurement of characteristic length of Nonlocal Continuuum », ASCE J. of Engrg. Mech., 115, n°4, 1989, pp. 755-767.

[BAZ 97] BAZANT Z.P., « Scaling of quasibrittle fracture: asymptotic analysis », Int. J. of Fracture, 83, 19-40 (1997).

[BOR 92] de Borst R., Muhlhaus H.B., « Gradient-dependent plasticity : Formulation and algorithmic aspects », *Int. J. Num. Meth. Eng.*, vol. 35, 1992, p. 521-539.

[BOR 96] DE BORST R., PAMIN J., « Gradient plasticity in numerical simulation of concrete cracking », Eur. J. Mech. A/Solids, 15, n° 2, 1996. pp. 295-320.

[EIB 93] Eible J. Lohrmann G., « Report on Subtask BE-89-3275 », University of Karlsruhe, 1993, 43 p.

[FEE 93] FEENSTRA P. H., « *Computational aspects of biaxial stress in plain and reinforced concrete* », PhD thesis : Delft Institute ot Technology, Netherlands, 1993, 149 p.

[FOK 92] FOKWA D., 'Materiaux Heterogenes: analyse experimentale et modelisation numerique par une approache hierarchique », Ph. D. Thesis, L.M.T.-Univ. Paris 6, 1992.

[FOK 93] FOKWA D., BERTHAUD Y., « Heterogeneous materials: experimental analysis of localization and the influence of size of heterogeneities on the behaviour in tension », Materials and Structures, 26, 1993, pp. 136-143.

[HIL 76] HILLERBORG A., MODEER M., PERTERSSON P.E., « Analysis of crack formation and crack growth in concrete by means of fracture mechanics and finite elements », *Magazine of Cement and Concrete Research*, 1976, Vol. 6, No. 6, p. 773 - 782

[HOR 91] HORDJIK D. A., « Local approach to fatigue of concrete ». Ph.D. thesis : Delft Institute ot Technology, Netherlands, 1991, 204 p.

[HUG 87] HUGHES T.J.R., *The Finite Element Method: Linear Static and Dynamic Analysis*, Printice Hall, New Jersy, 1987, 817p.

[LOD 94] LODIGOWSKI T., LENGNICK M., PERZYNA P., STEIN E., « Viscoplastic numerical analysis od dynamic plastic strain localization for ductile materials », *Arch. Rat. Mech. Anal.*, Vol. 60, 1994, p. 363-380.

[MEF 95] MEFTAH F., « Modélisation de la localisation dans les géomatériaux par la plasticité aux gradients : Element de poutre multicouches, *Rapport d'avancement de travaux de recherche* », LBS-INSA-Lyon, 1995, 95 p.

[MEF 97] MEFTAH F., « Contribution à l'étude numerique des modes localisés de rupture dans les structures en bétons de type poutre. approche multicouches par la plasticité au gradient », Thèse de Doctorat, INSA Lyon, France, 1997, 220 p.

[MEF 98] MEFTAH F., REYNOUARD J.M., « A multilayered beam element for gradient plasticity for the analysis of localized failure modes », *International Journal of Mechanics of Cohesive-Frictional Materials*, Accepted for publication September 97.

[MUH 91] MUHLHAUS H.-B., AIFANTIS E.C., « A variational principle for gradient plasticity », *Int. J. Solids Struct.*, 1991, Vol. 28, p. 845-857.

[NOO 92] NOORU-MOHAMED M.B., « Mixed mode fracture of concrete: an experimental approach », Ph.D.Thesis, Delft University of Technology, 1992.

[PAM 94] PAMIN J., « *Gradient-dependent plasticity in numerical simularion of localization phenomena* », Dissertation, Delft University of Technology, Delft, 1994, 134 p.

[PIJ 87] PIJAUDIER-CABOT G., BAZANT Z.P., « Nonlocal damage theory », *ASCE J. Eng. Mech.*, 1987, Vol. 113, p. 1512-1533.

[PRI 97] DI PRISCO M., FERRARA L., MEFTAH F., PAMIN J., DE BORST R., MAZARS J., REYNOUARD J.M., « Shear transfer in plain and reinforced concrete: capabilities of some

local and non-local models », Technical Report of ALERT Project 3.2, "Reinforced concrete", 1997.

[ROT 87] ROTS J.G. DE BORST R., « Analysis of mixed-mode fracture in concrete », ASCE, J. of Engrg. Mech., 113-11, 1739-1758 (1987).

[SAO 92] SAOURIDIS C., MAZARS J., « Prediction of the failure and size-effect in concrete via a bi-scale damage approach », Engineering Computations, ISSN 0264-4401, Swansea, UK, 9, 1992, pp. 329-344.

[SLU 92a] SLUYS L.J., « *Wave propagation, localization and dispersion in softening solids* », Dissertation, Delft University of Technology, Delft, 1992, 173 p.

[SLU 92b] SLUYS L.J., « Computational modelling of impact tests on steel fiber reinforced concrete beams ». *Comp. Mech. Compos. mat.*, 1992, Vol. 37, No 4, p. 3-15.

[SLU 94] SLUYS L.J., « Gradient theory : Discretization principles and application », *Proc. EURO-C 1994 Int. Conf. Computer Modelling of Concrete Structures*. Eds. H. Mang et al, Swansea : Pineridge Press, 1994, p. 403-412.

[SLU 95] SLUYS L.J., BRIOSCHI M.A., « Crack spacing in reinforced elements », In *Proc. Second Conf. on Fracture Mech. of Concrete Struc.* Ed. Wittmann F.H., Freiburg : AEDIFICATIO Publishers, 1995, pp. 1139-1153.

[SLU 96] SLUYS L.J., DE BORST R., « Failure in plain and reinforced concrete: an analysis of crack width and crack spacing », Int. J. Solids Structures, 33, 1996, pp. 3257-3276.